FATIGUE LIFE ASSESSMENT OF REELED RISERS

Theodoro Antoun Netto
Universidade Federal do Rio de Janeiro/ COPPE – Ocean Engineering Dept. – P.O. BOX 68508 – Rio de Janeiro/ RJ
tanetto@lts.coppe.ufrj.br

Marcelo Igor Lourenço
Universidade Federal do Rio de Janeiro/ COPPE – Ocean Engineering Dept. – P.O. BOX 68508 – Rio de Janeiro/ RJ
migor@lts.coppe.ufrj.br

Adriana Botto
Universidade Federal do Rio de Janeiro/ COPPE – Ocean Engineering Dept. – P.O. BOX 68508 – Rio de Janeiro/ RJ
adrianabotto@lts.coppe.ufrj.br

Abstract. *One of the most effective installation methods of metallic risers is the reel-lay process, in which pipe segments are welded onshore and subsequently bent over a cylindrical rigid surface (reel) in a laying vessel. During installation, the line is unreeld, straightened, and then laid into the sea under tension. In this process, material properties change and eventual weld defects may increase, thus reducing the fatigue life of those joints under operational loads. Therefore, welded joints must be manufactured based on strict weld acceptance criteria. These criteria shall guarantee reliable standards regarding the fatigue life of the joints while not impairing the feasibility of weld manufacture (high cost). In this work, the reeling process is initially simulated through a nonlinear finite element model that incorporates weld defects. The results are then used as guidelines to experimentally obtain fracture mechanics parameters of typical weld under pre-strained conditions. The fatigue life of as-welded and reeled joints with different defects (lack of fusion and lack of penetration) are subsequently estimated via a finite element model that accounts for the changes in the material properties due to prestraining. The results are compared and used to suggest guidelines to design of reeled steel catenary risers.*

Keywords*: reel method, fatigue life, SCR.*

1. Introduction

The most efficient and cost-effective method of pipeline installation involves pipe onshore welding and pipeline bending over a rigid circular surface on the vessel. During offshore installation, the pipeline is straightened and launched under tension into the sea. These methods have been successfully used in Brazil for installing pipelines up to 1,300 m (approximately 4,300 ft) water depth.

However, the bending, unbending, and straightening processes as applied on the vessels induce the pipe to bending-curvature histories, which are well into the plastic range of the material (e.g. Odegard et.al (1998)). Although the pipe is straightened prior to launch, distortions in the form of residual out-of-roundness, residual stresses, changes in material properties due to plasticity, and growing of eventual welding flaws may occur. These effects may have an influence in both the ultimate strength and subsequent fatigue performance of the line. Thus, in addition to ultimate strength design, the use of steel catenary risers (SCR's), which will be inevitably subjected to cyclic loading during operation, implies in a careful examination of the possibility of riser failure due to fatigue. In this context, the influence of installation methods involving pipeline material and geometric changes must be taken into account in the evaluation of the riser structural integrity during its operational life.

Fatigue life predictions based on S-N curves and fracture mechanics approaches can be employed in the preliminary stages of the design. Nevertheless, the necessary confidence to establish a consistent planning for SCR's installations using reel methods should be built upon laboratory fatigue tests using full-scale pipes and realistic girth welding processes. A test program including reeling simulation and fatigue tests on pipes with outside diameters (D) of 8.625 in and girth welds with induced lack of fusion and lack of penetration defects has been recently carried out at COPPE/UFRJ as part of a research project involving PETROBRAS and mostly funded by the Brazilian Governmental Financial Agency FINEP. The apparatus and the experimental procedures were described in a previous paper written by Netto, Lourenço and Botto (2004). The results obtained from the reeling experiments were first used to calibrate a three-dimensional nonlinear finite element model.

The model was then used to perform a series of calculations considering those two types of defects with different geometries. Guided by the experimental observations, attention was focused on the localized deformation that occurs in the vicinity of the defects during reeling. These results served as guidelines for the development of laboratory tests for determining fracture mechanics properties of raw and pre-strained test specimens made of typical weld. These include the resistance and da/dN curves. Finally, the fatigue lives of as-welded and reeled joints with different defects are calculated. A refined finite element model and, in parallel, fracture mechanics algorithms were developed with this purpose. The changes in the material properties due to pre-straining are incorporated in the analyses in order to verify their detrimental effect on the fatigue life of reeled pipes.

2. Experiments

The series of experiments on pipes of the material API 5l X60, with 8.625 in (2.08mm) external diameter, 0.593in (15.06mm) of thickness, 5.2m of length was described by Netto, Lourenço and Botto (2004) were used as a base case to develop the numerical analyses performed. The following nominal material and geometric parameters were employed: During manufacture, different discontinuities such as lack of fusion and lack of penetration (henceforth denominated LF and LP, respectively) were intentionally induced in the welds.

2.1. Material Parameters

2.1.1. Uniaxial Tension Tests

Three axial test coupons were cut from each pipe (base metal) used in the manufacture of the specimens. In order to determine the material parameters of the welds and the influence of the weld process in the material properties of the heat affected zone, a separate specimen with three girth welds was manufactured. Three sub sized specimens from each weld, three from each heat affected zone (HAZ) and three from the base metal (totaling twenty one specimens) were tested under uniaxial tension. These specimens were cut out in the hoop direction of 3 mm long rings sliced from cross sections coincident with each region. In addition, three axial test coupons from the base metal were tested. Figure 1 shows the average curves obtained for each region. In general, individual tests did not deviate more than 15% from the corresponding average. The yield stress in the hoop direction of the HAZ was in average 15% higher than in the base metal. Results also showed a weld overmatch of 20%. No significant differences were observed between the material parameters obtained in the axial and hoop direction of the base metal.

2.2. Fracture Mechanics Parameter Tests

As emphasized before, this work is focused on the evaluation of material pre-straining during installation and its detrimental effect in the fatigue performance of SCR´s. To this end, fracture mechanics parameters of weld were obtained experimentally for three different levels of pre-straining: 2.5%, 5%, and 7.5%. These levels were selected in light of the full-scale experiments and the numerical results that will be shown next.

The specimens were cut in the axial direction for the *da/dN* curve, while the Resistance curve had its coupons cut in the hoop direction. Pre-straining (tension) was applied in bar specimens made of raw material from welds. These were then used to make the actual three-point-bending specimens. Tests were performed in a servo-hydraulic machine equipped with a computerized data control and acquisition system. Initially, specimens were fatigue tested until a pre-crack of approximately 1 mm was formed. Crack extension was then monitored with the aid of a crack-opening-displacement (COD) gage sensor through the elastic compliance formulation. Specimen dimensions, test techniques, and fracture mechanics parameter calculations followed ASTM E-647 (2000) and E-1890 (1999) recommendations.

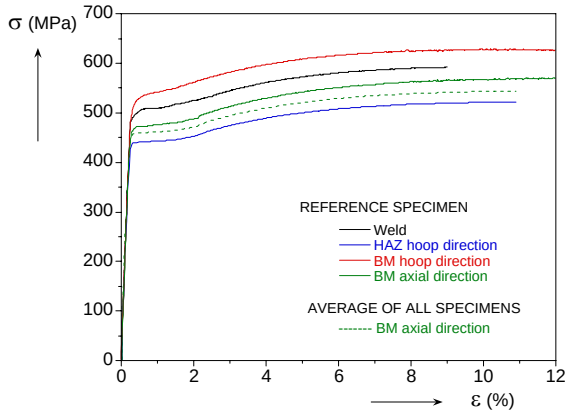

Figure 1. Uniaxial stress strain curves for weld, HAZ and base material.

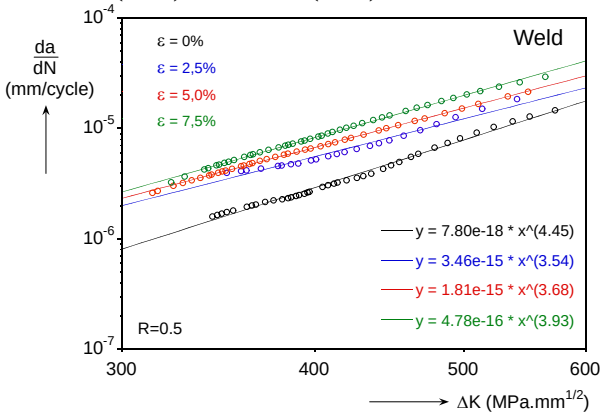

Figure 2. da/dN curves for weld raw for different levels of pre-strained material.

Figure 2 shows the *da/dN* versus stress intensity factor (ΔK) curves for the three levels of pre-straining, along with the corresponding raw material results obtained from the weld specimens. Noticeably, the effect is more pronounced for pre-strains less than 2.5%. As pre-straining is increased, the varied *da/dN* curves tend to coalesce. Paris law approximation (Eq. (1)) was fit to the individual sets of data. The parameters *C* and *m* are shown in graphic.

In another series of experiments, the Resistance curve was also obtained for different pre-straining levels. Due to the strain hardening, Kanninen (1985) defined the blunting line (Eq. (2)) as:

$$da/dN = C(\Delta K)^m \quad (1) \qquad \text{and} \qquad J = 2\sigma_y \Delta a \quad (2)$$

The blunting marks the beginning stage of material crack growth resistance development. The fracture toughness of the material can be interpreted as the initial stage of the material propagation. Figures 3.a and 3.b show the Resistance curves (J-integral and CTOD) for the different levels of pre-straining. Due to the small scatter and the little difference of the values obtained for J_Q e CTOD, the results obtained must be evaluated with some attention. It is know, by instant that there is a diminish tendency of fracture toughness parameters due to the pre-straining, being that not so significant for the material studied.

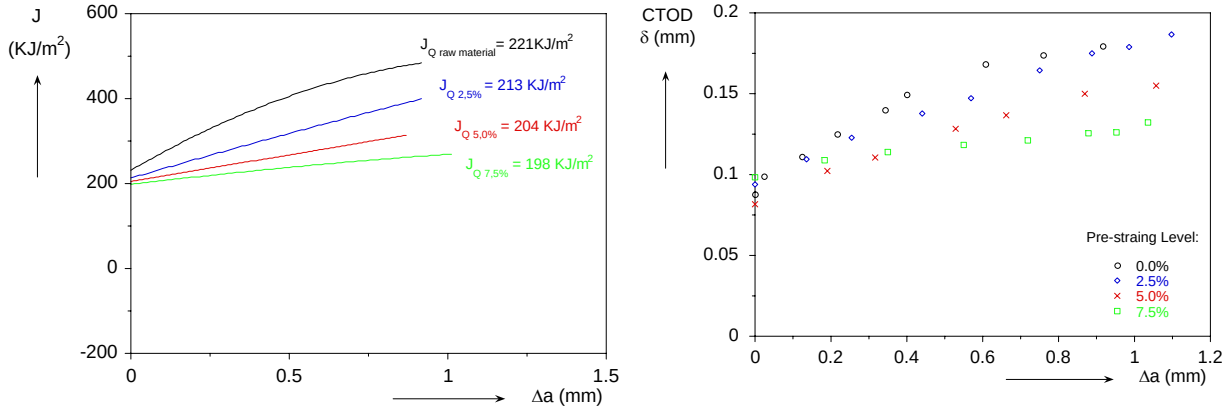

Figure 3.a and 3.b. Resistance Curves (J-integral and CTOD) for different levels of pre-straining.

3. Analyses

The experimental results were used to calibrate two three-dimensional nonlinear finite element models developed within the framework of ABAQUS version 6.3 (2003). One is able to simulate numerically the physical reeling experiments and the deformation mechanism in the weld region. A more complex model can reproduce initial cracks that are nucleated in the defect regions. It is employed to perform fracture mechanics analyses that are used, together with the material parameters obtained experimentally, to estimate the fatigue life of welded joints with different defects and pre-straining histories. Estimated the fatigue life was also compared with analytical predictions obtained with a specific algorithm developed using fracture mechanics simplified solutions.

The nominal pipe geometric parameter D = 219.08 mm and thickness (t = 15.06 mm) were adopted. Two types of defects were induced in the numerical model: lack of penetration and lack of fusion. The material parameters obtained for weld, HAZ and base metal shown in the previous section were used in the analyses. The longitudinal length of the HAZ was adopted equal to 2 mm in all cases studied.

Initially, the numerical models were used to simulate each of the physical experiments conducted (both reeling experiments and fatigue tests). The strains recorded in the reeling experiments were compared with the numerical results. In general, deviations from experiments fell within 20%. These differences were attributed to parameters such as weld material properties, initial out-of-roundness, thickness eccentricity, weld misalignment and residual stresses that may vary from specimen to specimen, but were not considered in the analyses for simplicity. Similarly, the fatigue-life predictions correlated well with the experimental results. In this case, a one to one correlation was avoided due to the natural variability in of fatigue test results. Nevertheless, and despite of the reduced number of experiments, the results evidenced a clear trend which was also reproduced by the model. The numerical and analytical procedures and a parametric study are presented next.

3.1. Reeling Analyses

A simplified model was used to reproduce numerically the pipe bending over a rigid surface and the deformation mechanism in the weld region. The pipe, including the defected weld region, was discretized with three-dimensional, 20-node, quadratic brick elements (C3D20). The number of integration points per element was 20, i.e., a full integration scheme was used. An overall view of the model, including pipe and the reel rigid surface with radii of curvature equal to 6 m, is shown in Fig. 4. The pipe length (L) was set equal to 5.2 m (the same as in the experimental tests). Figure 5 (a) and (b) show in detail the mesh in the neighborhood of both LP and LF defects. Forty one elements in the axial direction, twenty two in the circumferential direction and seven through the thickness were adopted after convergence tests and mesh sensitivity analyses. The actual mesh distribution varied slightly for each analysis depending on the geometry of the defects, though roughly keeping the same total number of elements.

The deformation of the cross-sections of the pipes is assumed to be symmetric with respect to plane 1-2. Furthermore, plane 2-3, located at the mid axial position of the pipe (and defect), and is also assumed to be a plane of symmetry. Contact between pipe and reel was simulated by using surface-based hard-contact modeling. This model prevents penetration between contact surfaces. Pipe and welds were assumed to be J_2–type, elastic-plastic, finitely deforming solids with isotropic hardening. Bending over the reel is performed with the aid of a reference node at

$x_1=x_2=x_3=0$ that is coupled with the edge nodes on plane 2-3 at $x_1=0$. A kinematic coupling constraint makes the set of edge nodes to follow the rigid body motion of the reference node. Therefore, the pipe is deformed against the reel by setting increments of displacement in the x_2 direction at the reference node.

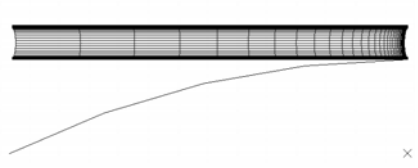

Figure 4: Overview of mesh used for the reeling.

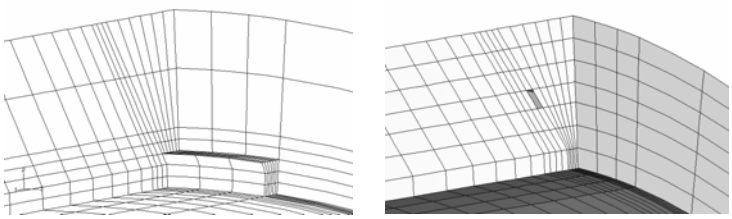

(a) (b)

Figure 5. Typical mesh in the vicinity of (a) LP and (b) LF defects.

BS-7910

The Failure Assessment Diagram (FAD) is based on principles of fracture mechanics, where the horizontal axis correspond to a plastic collapse parameter and the vertical axes is a fracture ration. Calculations for a flaw provide its co-ordinate point or locus of point. The level 2B and 3B of the Failure Assessment Diagram were considered. The main difference between the two approaches is the data available and the conservatism required; therefore level 3B includes a more accurate procedure for ductile tearing evaluation. For this type of analysis, the fracture tearing resistance is defined as a function of the amount of ductile crack extension, i.e. the R-curve. The FAD cut-off is to prevent localized plastic collapse and is taken as the average of the yield strength and the tensile strength normalized by the yield strength.

Figure 6 and 7 shows the results of the FAD for different sizes of defects ((a/t (FP) or 2 a/t (FF) equal to 0.066, 0.1328, 0.1992, 0.2656 e 0.3320). For level 2B, all the LP defects were considered not acceptable, as greater the size of the defect, more distant the point is plotted from the curve (where the acceptable levels are). For level 3B, all the defects were considered valid unless LP = 5mm. Analyzing the results obtained for the two types of defect, it is clear that the LP defect is considered more critical then the LF defect. All the LF defects in both levels of evaluation were considered acceptable.

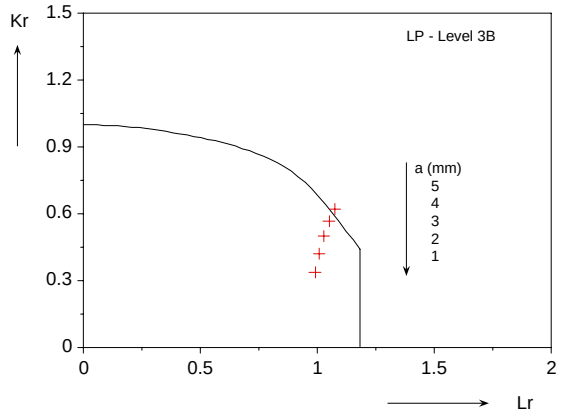

Figure 6. FAD, Level 3B – LP defects.

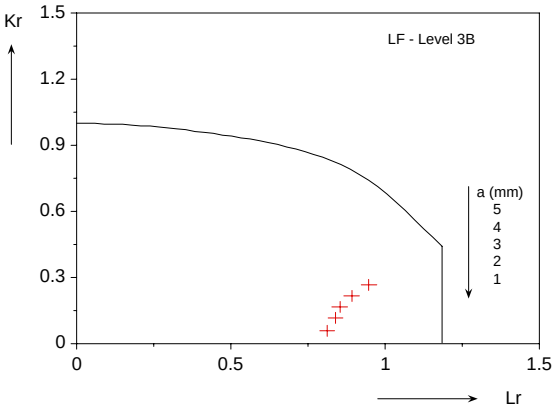

Figure 7. FAD, Level 3B – LF defects.

Reel Parametric Study

Through a good correlation and the results obtained by the analytical study based on the BS-7910, a parametric study was performed in order to estimate the magnitude of the localized strains experienced in the vicinity of the defects during reeling, in which the type of defects and their dimensions were varied. For each type of defect (LP and LF), three heights were considered, a/t (LP) or $2a/t$ (LF) equal to 0.1328, 0.1992 and 0.2656 (i.e., 2, 3 and 4 mm), while the length c was set equal to 20 mm (c/D = 0.0913). Defects were positioned so to coincide their middle with the angular position of maximum tensile longitudinal bending strains (bending plane). Additionally, the middle of LP defects was located at mid-thickness.

The results corroborate the experimental findings that for a given angular position, the local strain history varies depending on the region (weld, HAZ, and base metal) and type of defect. More importantly, these strains change significantly through the thickness. Figures 8 and 9 depict the longitudinal strains experienced in the bending plane along two paths. For LP cases, the maximum strains corresponding to a/t = 0.1328, 0.1992 and 0.2656 were 5.9%, 6.3% and 8.2%, respectively (path 1). Calculated maximum strains along path 1 for the three LF defects were 2.1%, 2.9% and 3.9%. The three different levels of pre-straining: 2.5%, 5%, and 7.5% were selected in light of the full-scale experiments and the numerical results. As shown previously, these levels of pre-straining affect the material fracture

mechanics parameters (specifically *J-R* and *da/dN* curves), and, in turn, deteriorate the fatigue performance of the welded joint.

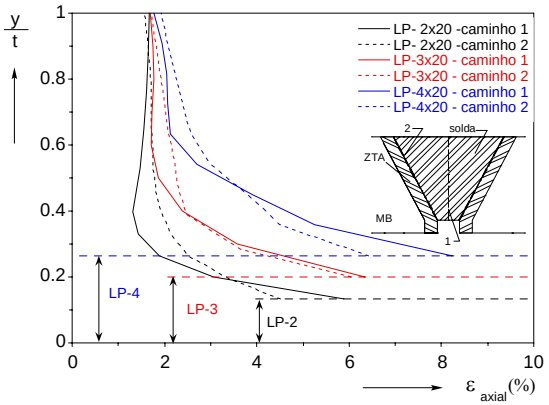

Figure 8. Longitudinal strains experienced in the bending plane along two paths for a LP defect.

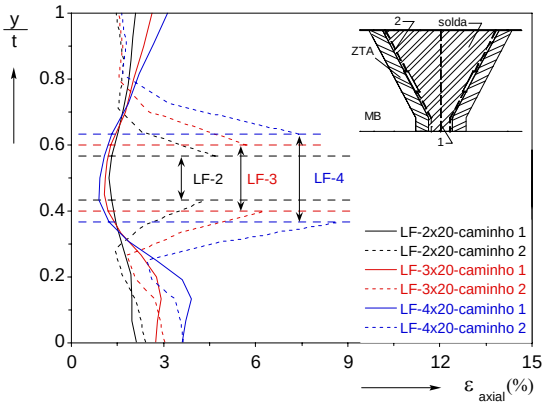

Figure 9. Longitudinal strains experienced in the bending plane along two paths for a LF defect.

3.2. Fatigue Analyses

3.2.1. Fatigue Finite Element Analysis

A fracture mechanics approach was used to estimate the fatigue life of the welded joints. LP and LF defects were considered as crack initiation sites and the stress intensity factors along their edges were calculated with the aid of a linear elastic finite element model (i.e., small scale yielding is assumed). Again, 20-node, quadratic brick elements (C3D20) were used, but a much more refined mesh was needed due to the resulting singular stress state at the crack tips. This was obtained by collapsing together two edges of the elements around the crack tips. The node distribution of these elements is such that their mapping to a fixed master element generates a singular stress field around the crack tips. The resulting singularity is of the form $1/\sqrt{r}$, where r is the radial distance of a given point with respect to the crack tip.

The geometric parameters and symmetry conditions are identical as the model used in the reeling analyses, though here the pipe length was only twice the nominal diameter. This reduced length was considered enough to apply the edge loading without affecting the stress field at the weld region.

The curved shape at the weld root was intentionally made to better reproduce the actual cases. In the experimental tests it was observed that, in the case of LP defects, cracks nucleate at either side of the lower boundary between weld material and HAZ (e.g. Netto, Lourenço and Botto (2004)). Thus, singular elements were placed around this region for the calculation of the stress intensity factor. For LF cases, singular elements were placed around the top and bottom of the defect, i.e., the defect was treated as an initial crack itself. Figures 10 and 11 show details of typical meshes used for both cases.

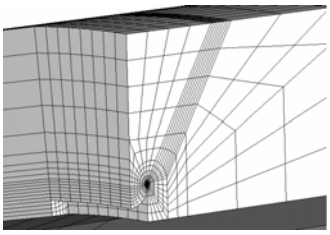

(a)

Figure 10. Detail of the LP defect region.

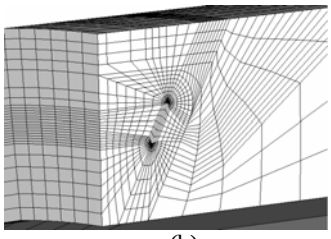

(b)

Figure 11. Detail of the LF defect region.

As in the previous model, the edge nodes are kinematically coupled to a reference node at $x_1=x_2=x_3=0$. Full-reversed cyclic bending load is then applied on the pipe by prescribing bending load on the reference node. Five stress ranges away from the weld region were considered: 50, 78, 110, 190 and 300 MPa.

A *J*-integral formulation is used to calculate the stress intensity factor at the crack tips. For the sake of space the detailed procedure will not be provided here. Interested readers are referred to the Abaqus Theory Manual (2003) for further details on this subject. For a given stress range, fatigue crack growth and number of cycles until failure (N_f) were evaluated in a simplified manner, as follows: The stress intensity factor range (ΔK) is calculated considering the initial crack size (in the analyses, we considered $a_0=2$ and 3 mm for LP and $2a_0=2$ and 3 mm for LF). We assume $\Delta K = \Delta\sigma\sqrt{\pi a}Q$ where the function of geometry Q is independent of the crack size a. This approximation was deemed

reasonable (Netto, Lourenço and Botto (2004)). By integrating Paris Law equation, it is possible to make a quantitative prediction of the number of cycles until failure.

The maximum allowable crack size is 0.8t. In any case, we assume that if this dimension of crack is reached, the residual number of cycles until failure is relatively very small, due to increasing plastic deformation ahead of the propagation front (ductile tearing).

3.2.2. Fracture Mechanics Algorithm

Based on analytic formulations, developed for elliptical and semi-elliptical flaws, the variation of the SIF during the crack propagation can be assessed. These formulations are able to take in account the stress variation through the pipe thickness. An algorithm was developed using the solutions for the factor of geometry obtained from the API-579 and BS-7910 standards. The solutions for semi-elliptical and elliptical cracks are obtained from handbooks and numerical modeling of curved shells.

Flaw Characterization

Flaw characterization rules allow existing or postulated crack geometry to be modeled by a geometrically simpler one in order to make the actual crack geometry more amenable to fracture mechanics analysis. The rules are necessarily conservative and intended to lead to idealized crack geometries that are more severe than the actual crack geometry they represent. Figure 12 shows the general procedure used on the characterization of surface and embedded flaws. This procedure results on simplified dimensions for the lack of penetration and lack of fusion weld defects.

In general, the crack length is easy to be obtained. If the flaw is oriented perpendicular to the plane of the maximum principal tensile stress in the component, then the flaw length to be used in calculations is merely the one measured with non-destructive tests. However, if the flaw does not lie in a principal plane, then an equivalent flaw dimension with a mode I orientation shall be inferred. The more adequated procedure, recommended by both standards, consists on projecting the flaw onto the plane of the maximum principal stress. In case of uncertainty about which principal direction will be used (biaxial load), both directions should be analyzed in order to determine the critic one.

The length and depth of the lack of penetration defects are perpendicular to the axial direction. However, the depth of the lack of fusion defects is not aligned with the radial direction, since this defect lies on the bezel wall. So, a relative defect depth, referred to the mode I, was calculated for the lack of fusion defect.

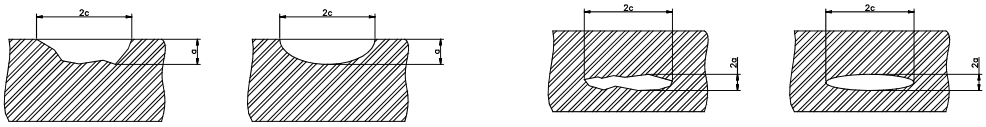

(a) (b)

Figure 12. (a) surface and (b) embedded defect characterization.

Stress Intensity Factor (SIF)

Analytical solutions for SIF calculations of elliptical and semi-elliptical cracks are well documented in the literature (Newman and Raju (1984)). Nevertheless, these solutions are presented for two cases of stress distribution through the thickness: uniform and linear. BS-7910 and API-579 standards bring a compendium of tabled solutions for the geometry factor considering a large range of relation between axes of the ellipse.

In the case of tubular welded structures, situations as misalignment, thickness variations, residual stresses and the material properties variation on the welded region may lead to a more complex stress variation through the thickness. These stress distribution can be obtained using numerical models or empirical and semi-empirical formulations.

The weight functions proposed initially by Bueckner (1970) and studied by Rice (1972) helps to deal with these complex stress state. Consider a complex stress distribution represented by $\sigma(x)$. Once obtained the weight function $h(x,a)$, which is a function of geometry and dimensions of the crack, it's possible to calculate the SIF for mode I integrating by Eq. (4):

$$K_I = \int_0^a h(x,a)\sigma(x)\,dx \qquad (4)$$

In the case of surface cracks with semi-elliptical shape in cylinders, Shen e Glinka (1991) presents the solution for the weight functions used in the algorithm. Regarding the embedded flows, the solutions of Sih (1977) were used.

Flow recategorization

Flaw recategorization is required for two situations: when an embedded flaw, during its propagation, reaches a region close to the surface. The algorithm recategarize it as a surface flow; or when a deep surface flaw presents a small remaining ligament. In this case, the algorithm recategorize it as a through-wall flaw.

The assumed flaw dimensions are modified as follows. An embedded flaw should be recategorized to a surface flaw when $d/t < 0.2$ (see Fig. 13.a). The length and depth of the surface flaw are given by Eq. (5):

$$2c_s = 2c_i + 2d \qquad a_s = 2a_i + d \qquad (5)$$

A surface flaw should be recategorized as a through-thickness flaw when *a/t > 0.8* (see Fig. 13.b). The length of the through-wall flaw is given by Eq. (6):

$$2c_p = 2c_s + 2\left(t - a_s\right) \qquad (6)$$

Note that the crack length is increased in each case by twice the ligament dimension. When the plastic strain on the remaining ligament is large, the flaw could grow to the free surface by ductile tearing, in which case the flaw might also extend in the length direction.

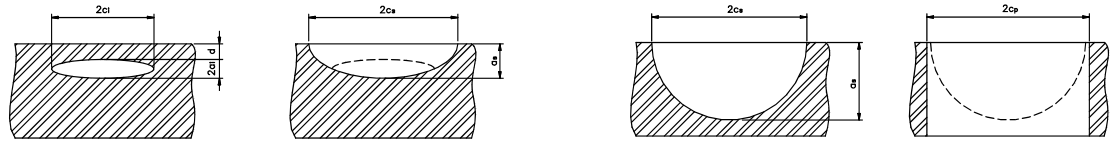

(a) (b)

Figure 13. (a) embedded and (b) surface flow recategorization

Algorithm development

FORTRAN 95 was used to develop the algorithms. The applications were then compiled as Windows Dynamic Link Libraries (DLL). A friendly interface was structured using DELPHI 7. This interface allows the user to visualize and change the analysis necessary variables, follow the fatigue life calculation process and check the final results of the analysis. The application developed using DELPHI interacts with the algorithms developed using FORTRAN and storied in the libraries. The following steps describe the application operation. The user enters with the defect type, initial dimensions of the defect and the pipe dimensions. Then the fatigue propagation law parameters most be provide. The algorithm integrates numerically the Paris law. During the numerical integration, crack dimensions and the SIF value are recalculated at each cycle, i.e., at each cycle, the SIF is calculated and the weight functions (Eq. (7)) are used to extend this calculation to a complex stress state as described. The number of cycles is computed until the crack becomes through-wall. The conditions to crack recategorization are checked at each cycle and, if necessary, the procedures described (Eq. (5) and (6)) are applied. The parameters of a forth degree equation may be provided to represent the stress variaton *σ(x)* through the thickness as follow.

$$\sigma(x) = \sigma_0 + \sigma_1\left(\frac{x}{t}\right) + \sigma_2\left(\frac{x}{t}\right)^2 + \sigma_3\left(\frac{x}{t}\right)^3 + \sigma_4\left(\frac{x}{t}\right)^4 \qquad (7)$$

3.2.3. Fatigue Parametric Study

A parametric study was performed with typical defects of lack of fusion and lack of penetration. Both numerical model and algorithm were used and compared. This study also contributes to understand the effect of material pre-straining of the welded joints fatigue life. The same 8 inches pipe mentioned in item 2 was modeled and two defect dimensions were considered: lack of fusion with 2 and 3 mm depth and 20 mm length and lack of penetration also with 2 and 3 mm depth and 20 mm length. Five different levels of load were applied: 50, 78, 110, 190 e 300 MPa. Additionally, mean stress ($R = \sigma_{min}/\sigma_{max} = 0,5$) was considered so as to avoid compression of the crack faces throughout the cyclic load. The numerical results are summarized in Fig. 14 - 15. As reference, they are plotted in S-N diagram format together with design curves currently used in practice.

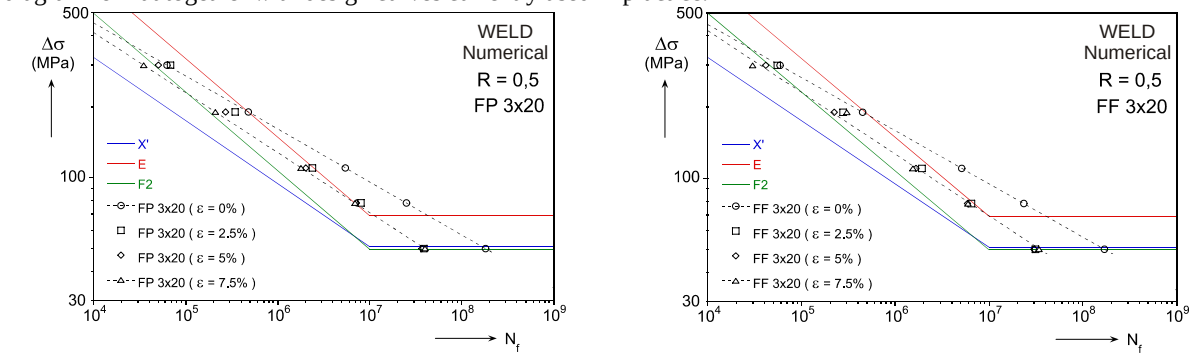

Figure 14. S-N curves obtained with numerical modeling

The effect of material pre-straining is illustrated in Fig. 14 (numerical models) and Fig. 15 (algorithm). The detrimental effect on the fatigue performance due to the deterioration of the fracture mechanics properties is clear, specially for lower values of $\Delta\sigma$. For example, the numerically calculated number of cycles until failure for $\Delta\sigma = 190$ MPa using raw material properties is 7.89×10^6. For 2.5%, 5% and 7.5% this value drops 36,8%, 49,3%, e 59,2% respectively. The corresponding relative reductions in fatigue lives for $\Delta\sigma = 78$ MPa are 72,5%, 75,0% e 76,8%. For better comparison, dashed lines were fit to the data corresponding to raw and 7.5% pre-strained material. The figures

show small difference between the two models. For instance, if we calculate the fatigue life drop for $\Delta\sigma = 78$ MPa using now the algorithm, the obtained values will be 71,4%, 74,6% e 76,2%. These values are very close to the ones obtained numerically.

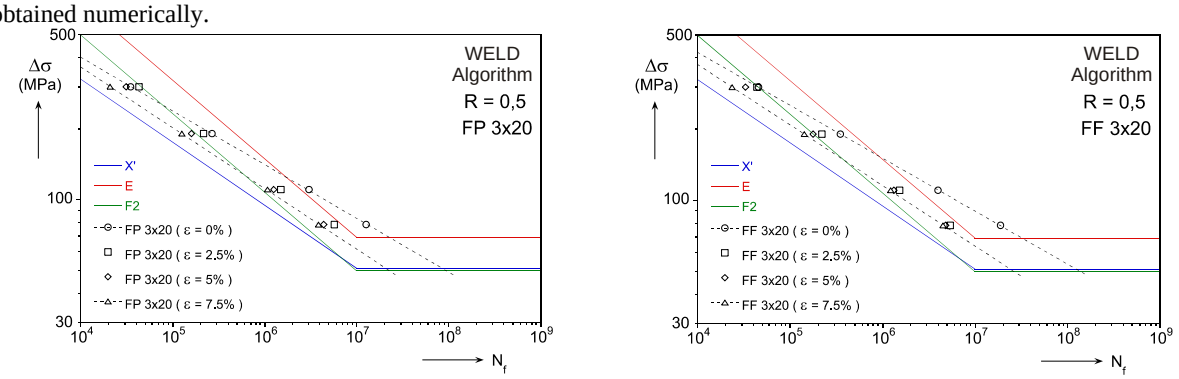

Figure 15. S-N curves obtained using the algorithm

4. Conclusions

The fatigue performance of reeled risers has been studied through combined experiments and analyses. Full-scale experiments, FE and analytical calculations of the types described above are viable options. FE calculations and analytical modeling have shone similar results, proving that the algorithm is a good project tool. Approximate S-N design curves such as the ones considered in this study are very useful for parametric studies when the problem parameters are yet not well defined. Their use in the case of SCR installed by the reel method was dubious, however, due to the uncertainty related to the detrimental effect of material pre-straining in the fatigue performance of the welded joints. In order to elucidate this issue, fatigue life results for varied stress ranges obtained numerically were compared with three S-N curves used in practice (E, X´ and F2). Depending on the defect, stress range, mean stress, and pre-straining, curve E may underestimate or overestimate the fatigue life as compared with the numerical results. In all cases, curves X´ yielded conservative estimates. These can be thus considered dependable design tools for reeled SCR´s, provided the problem parameters do not deviate significantly from those contemplated in this study.

5. Acknowledgements

The experimental work was conducted with the financial support from FINEP-Brazil and a consortium of industrial sponsors. The work of T.A. Netto, Lourenço and Botto was also sponsored by CNPq-Brazil, and that of M.I. Lourenço and A. Botto by ANP-Brazil. The authors would like to thank the technical staff of the Submarine Technology Laboratory – COPPE/UFRJ for the assistance in the design and execution of the experiments.

6. References

ABAQUS User's Manual (2003). Version 6.3, p.7.9.1, Hibbit, Karlsson and Sorensen, Inc.
API RP 2A (1991). Planning. Designing and Constructiong fixed Offshore Plataforms.
ASTM E-647 (2000), Standard Test Method for Measurement of Fatigue Crack Groths Rates.
ASTM E-1890 (1999), Standard Method for Measurement of Fracture Thoughness.
DNV Classification Notes (1984), Note No 30.2, Fatigue Strength Analysis for Mobile Offshore Units.
Kanninen, M. V. F e Popelar, C. H., 1985 – Advanced Fracture Mechanics, Oxford University Press, Nova York.
Miscow et al (2003), Techniques to characterize fatigue behavior of full size drill pipes and small scale samples, *International Journal of Fatigue.*
Netto, T.N, Lourenço, M.I and Botto, A (2004). Fatigue performance of reeled pipes. Proc. 22nd International Conference on Offshore Mechanics and Arctic Engineering.
Odegard, J., Taulow, C., Haisen, K., and Barde, M. (1998). Installation of titanium pipelines by reeling strain analysis and material properties. *Proc. 17th International Conference on Offshore Mechanics and Arctic Engineering*.
Silk, M.G. (1978), New Approaches to Crack Sizing by Ultrasonics – Recent Developments in Non-Destructive Testing, *Seminar papers*, Abington, Cambridge, Oct. 1976, Published by the Welding Institute, paper 5, pp.40-45.
Newman, J.C., Raju, I.S., (1984), Stress Intensity Factor Equations for Cracks in Three-Dimensional Finite Bodies Subject to Tension and Bending Loads, NASA Technical Memorandum 85793.
Bueckner, H.F., (1970), A novel principle for the computation of stress intensity factors, ZAMM, Vol. 50, pp. 529-546.
Rice, J.R., (1972), Some remarks on elastic crack-tip stress fields, Int. J. Solids Structures, Vol. 8, pp. 751-758.
Shen, G., Glinka, G., (1991), Weight Functions for a Surface Semi-Elliptical Crack in a Finite Thickness Plate, Theoretical and Applied Fracture Mechanics, Vol 15, pp. 247-255.
Sih,G.C., (1977), Mechanics Of Fracture 3, Plates and Shells with Cracks, Noordhoff International Publishing Leydon, The Netherlands.